FISEVIER

Contents lists available at ScienceDirect

# Journal of Drug Delivery Science and Technology

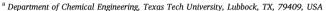
journal homepage: www.elsevier.com/locate/jddst



# Research paper

# Feasibility of using negative pressure for jet injection applications

Yatish S. Rane <sup>a</sup>, James B. Thomas <sup>a</sup>, Paul Fisher <sup>b</sup>, Kate E. Broderick <sup>b</sup>, Jeremy O. Marston <sup>a,\*</sup>



<sup>&</sup>lt;sup>b</sup> Inovio Pharmaceuticals, 10480 Wateridge Circle, San Diego, CA, 92121, USA

#### ARTICLE INFO

Keywords: Needle-free injection Liquid jet Negative pressure

#### ABSTRACT

We report on an experimental study of high-speed micro-scale liquid jets ejected into low-pressure environments, which has applications for the use of negative pressure modules in jet injector systems. The jets were impulsively started by the action of a stiff spring-piston and ejected through a narrow orifice,  $D_0 \sim 100~\mu m$ , into partial vacuums ranging from atmospheric pressure down to -80~kPa. We find that due to the high exit velocity,  $v_j \sim 100~m/s$ , the main jet stream is largely unaffected, but we reveal some fascinating fine features during the start-up phase, largely due to the presence of a small liquid volume pulled through the orifice prior to actuating the jet. In particular, as the pressure decreases, the start-up time increases and the initial spray becomes more pronounced. However, the primary outcome of this feasibility study is that use of negative pressures is viable for jet injector applications, and we hypothesize an optimal range of working pressures and configurations.

#### 1. Introduction

Routine administration of vaccines via hypodermic needle and syringe is known to cause mild to severe anxiety in patients with needle-phobia (trypanophobia), and affects approximately one in ten patients in the US [1–3]. Combined with the risk of contamination from hazardous sharps waste [4,5], and cost of treating accidental needle-stick injuries [6,7], the Safe Injection Global Network (SIGN) and Global Vaccine Action Plan (GVAP) of the WHO have therefore in the past recommended the development of needle-free injection technologies, noting that they reduce the risk of spreading infection [8–11]. In addition, there have been promising developments for a technique known as fractional dose vaccination, where a small dose (typically 1/10th - 1/5th of a standard dose) is delivered into intradermal tissues. Multiple studies [12–17] now prove that this technique is feasible for mass immunizations, which as shown by the recent pandemic, are going to be vital for forseeable future.

Whilst jet injectors were originally proposed as a candidate to replace needles for standard intramuscular injections [18–22], they also clearly hold promise for fractional dose vaccine delivery [12–17], and there have been numerous studies assessing both the fundamental mechanics [23–47] and clinical success [12–17,48–51] of needle-free jet injection. The basic premise is that a high upstream pressure, created using either a spring or compressed gas mechanism, forces a jet at high-speed,  $v_{iet}$   $\sim$ O(100 m/s), from a narrow orifice,  $D_0$   $\sim$ O(100  $\mu$ m).

Studies with both commercial and custom devices in the literature have comprised a range of in-vitro, ex-vivo and in-vivo systems, however there is considerable variability in terms of injection efficiency, i.e. the ratio of drug delivered to intra-dermal region of skin to the amount of drug in cartridge. One hypothesis is that the skin tension, underlying tissue stiffness, and position relative to the jet orifice play a key role in achieving a consistent jet injection [52,53]. To exemplify this, Fig. 1 provides a direct comparison of a jet injection administered into Guinea pig skin with a solid backing that fixes the skin position (a & b), and an injection where no solid backing (natural tissue) is implemented (c & d). It is clear that the force of the jet is sufficient to significantly deflect the skin. This leads to inconsistent (and failed) injections.

In order to circumvent this inherent variation, devices have been proposed in which a negative pressure module could be placed against the skin prior to administering the jet injection [54–57]. However, to date, there have been no studies in the literature of the feasibility of this approach. Therefore, the specific goal of this study was to determine the feasibility of using a jet injector in partial vacuum, i.e. can we achieve a steady jet stream and drug delivery into skin? In particular, does the jet perform consistently over a broad range of pressures and viscosities? To answer this question, we used high-speed videography to capture jet dynamics for fluid viscosities spanning three orders of magnitude and pressures from 0 to  $-80\ kPa$ , and performed a limited set of ex-vivo trials using Guinea Pig skin.

E-mail address: jeremy.marston@ttu.edu (J.O. Marston).

<sup>\*</sup> Corresponding author.

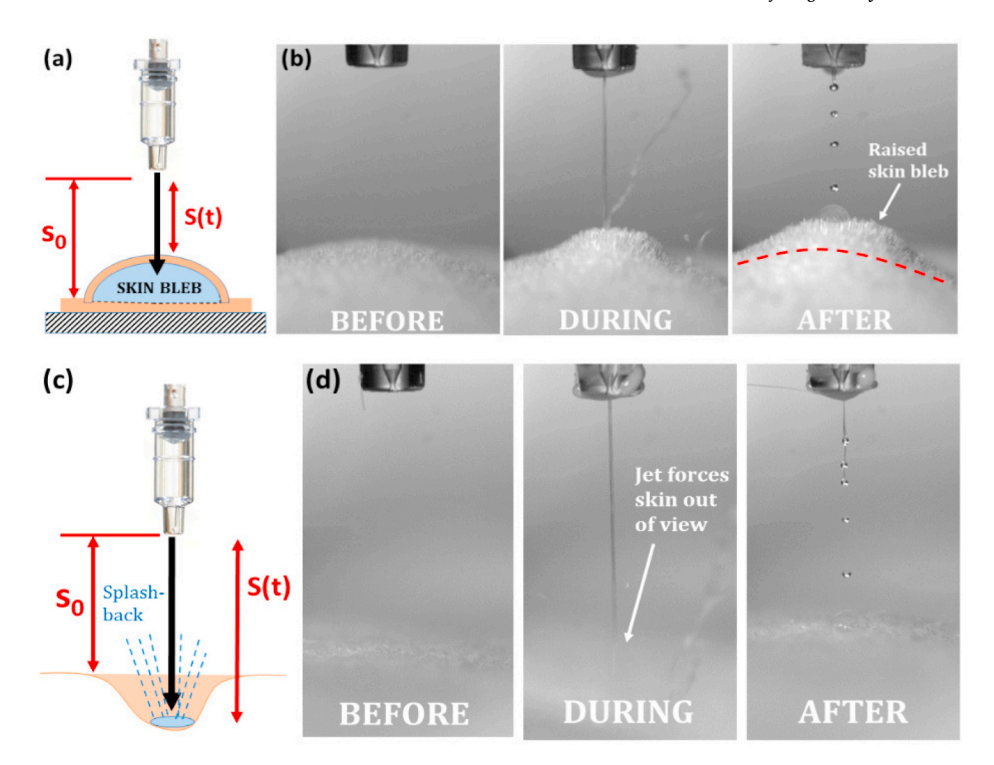


Fig. 1. Comparison of jet injections (0.1 mL) into guinea pig skin with a solid backing (a & b) and soft tissue backing (c & d). The solid backing leads to a successful intradermal injection and skin bleb formation, whilst the soft tissue backing results in skin delfection, splashback and a failed injection.

## 2. Experimental methods

The jet injector used in this study was the Bioject ID Pen [45–47,64], which is a streamline (narrow profile) device originally designed for intradermal injection purposes. The device, shown in Fig. 2(a), comprises a spring housed in an upper chamber which is cocked by manually extending the arm on the outside of the chamber. A cartridge, shown in Fig. 2(b), pre-loaded with fluid is then inserted into the front end of the device and locked in place by rotation. The injection is then triggered manually by pressing on an external trigger ring, whereupon the spring is released and a piston hits the rear end of the plunger. After the injection, the used cartridge is released from position by pulling on a release ring.

The vacuum chamber, shown in Fig. 2(c), is made of 3/4-inch acrylic, and is de-pressurized using a hand vacuum pump for fine control of the pressure, which is read using a digital vacuum gauge. The depressurization takes several seconds, and the only part of the injector that is in contact with the negative pressure is the orifice of the cartridge. Therefore, the main injector assembly (Fig. 2(a)) is unaffected by the process.

The cartridges expel a total volume of 100  $\mu$ L (actual capacity is slightly higher to account for dead volume in the conical taper section). The upper cartridge inner diameter where the plunger travels is  $D_p=4.57$  mm, whilst the orifice diameter from where the jet exits is  $D_0=157$   $\mu$ m. By tracking the plunger displacement and applying mass conservation, the exit velocity at the orifice was found to vary from 161 m/s for water down down to 74 m/s for glycerin, thus yielding jet Reynolds numbers,  $Re_i=\rho v_i D_0/\mu=1.1\times 10^1$  up to  $2.5\times 10^4$ .

For this study, a range of water-glycerin mixtures were studied with the percentage of glycerin concentration (measured by weight) varying from 0 to 100  $\%_{w/w}$ . Note that we did not consider concentrations below

50% since the difference in viscosity is very small in that range. The viscosity was determined using a stress-controlled protocol on a TA DHR3 rheometer with a 40 mm, 0.017 radian cone-and-plate geometry. Multiple measurements for each fluid were performed at a constant temperature of 20  $^{\circ}\text{C}$ . The summary of fluids used is shown in Table 1 (Newtonian).

To capture the jet dynamics, we employed high-speed video cameras (Phantom V1611 and V711) from Vision Research Ltd. For most cases, a single side-view perspective was sufficient to measure the plunger displacement, which is used to calculate the instantaneous plunger velocity, from which we can derive the flow rate and instantaneous exit (jet) speed. However, in some cases, we employed two cameras with orthogonal views to obtain a better understanding of jet dispersion patterns. The cameras were operated at frame rates up to 100,000 fps, but typical video sequences were captured at 20,000 fps. The temporal resolution is therefore  $\pm 50~\mu s$ , which is factored into our errors when calculating jetting times. In addition, using Nikon micro-nikkor 60 mm lenses with extension tubes, we achieved typical effective pixel sizes of between 16 and 50  $\mu m/px$ .

## 3. Results and discussion

#### 3.1. Overview

As a general overview to the effect of both vacuum pressure and viscosity on the jet start-up and stream collimation, we present Figs. 3 and 4 which show image sequences from high-speed video clips. In both figures, sequences (a) and (b) are taken at P=0 and P=-80 kPa, respectively, and we clearly observe the qualitative effect of the negative pressure. For water, the presence of a pendant drop leads to a spray of droplets when the impulsive action of the spring-piston commences.

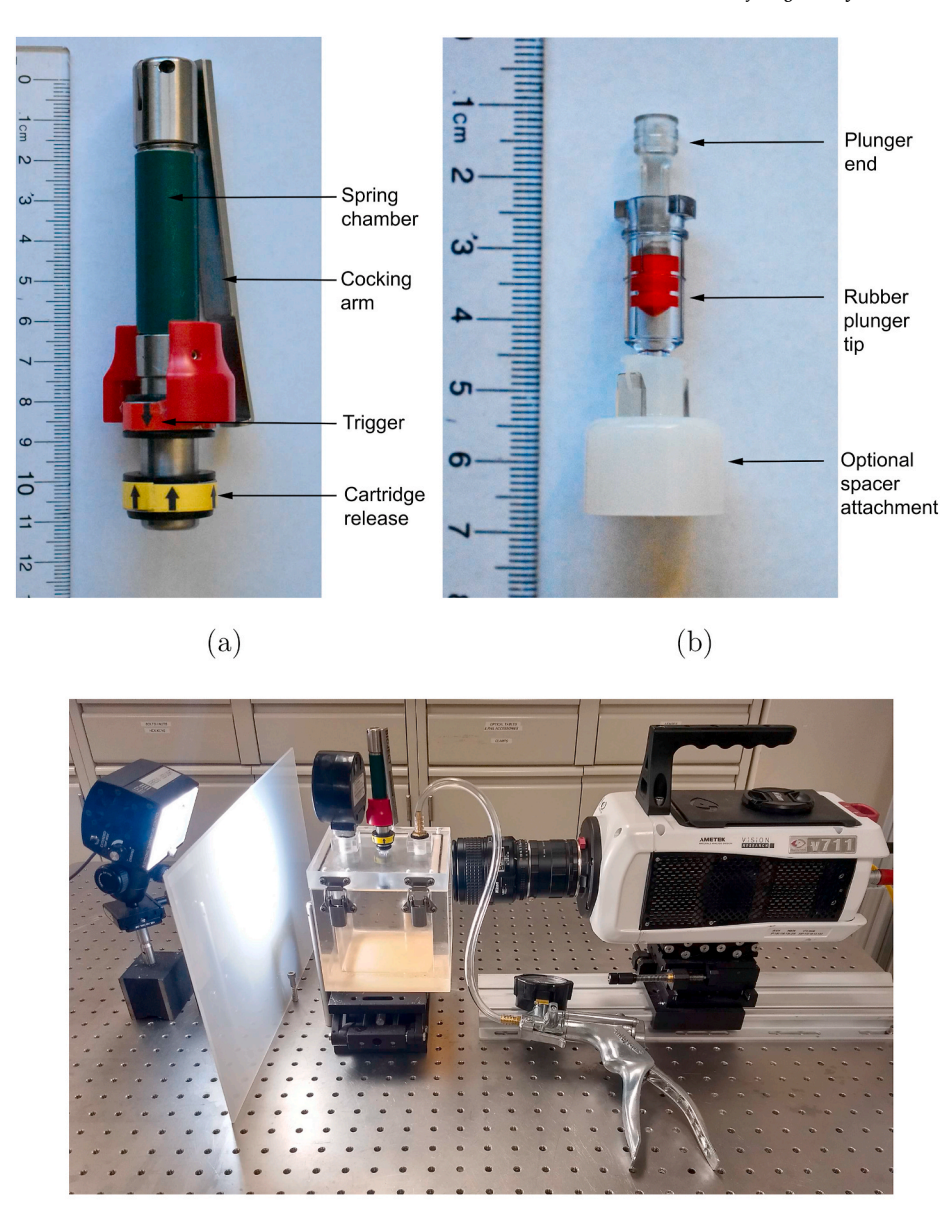


Fig. 2. Photographs of (a) the ID Pen device and (b) standard cartridge for ejecting a volume of 0.1 mL. The white spacer attachment at the end of the cartridge featured in (b) is optional to create a stand-off distance of approximately 16 mm. (c) Photograph of the experimental setup, showing the vacuum chamber with ports for vacuum line and gauge.

(c)

**Table 1**Physical properties of the liquids used in the experiments. The glycerol mixtures are stated as concentration by volume.

Liquid	Dynamic viscosity $\mu$ (Pa.s)	$\frac{\text{Density}}{\rho \text{ (kg/m}^3)}$
50% glycerol	0.0069	1130
80% glycerol	0.084	1209
90% glycerol	0.215	1235
95% glycerol	0.482	1248
100% glycerol	1.31	1261

These droplets gradually disperse away from the orifice over the first 10 ms of the jet. This drop is the result of fluid volume pulled through the orifice during depressurization of the chamber, and is a consistent feature, as evidenced in Fig. 4(b) for glycerin - here however, it does not

lead to a spray, but an elongation of the pendant drop, which takes more time to clear away from the orifice. For both fluids, the negative pressure ultimately leads to a more dispersed and angled jet, with a deflection angle (from vertical) of approximately 4°.

## 3.2. Fine features of the jet start-up

The high-speed videos reveal a relatively fast start-up and transition to steady, collimated jet stream for jets emerging into atmospheric pressure, such as those shown in Figs. 3(a) and 4(a). However, the jets emerging into negative ambient pressure are subject to the presence of a pendant drop, which is an inevitable consequence of the system at hand. To study the formation of the steady-stream jet in such cases, we present Figs. 5 and 6, for water and higher-viscosity fluids, respectively.

In Fig. 5(a), the images reveal intricate details of the pendant drop atomization; the high-speed jet punctures through the drop at the apex (image 2) and causes a fine spray of droplets moving rapidly downward

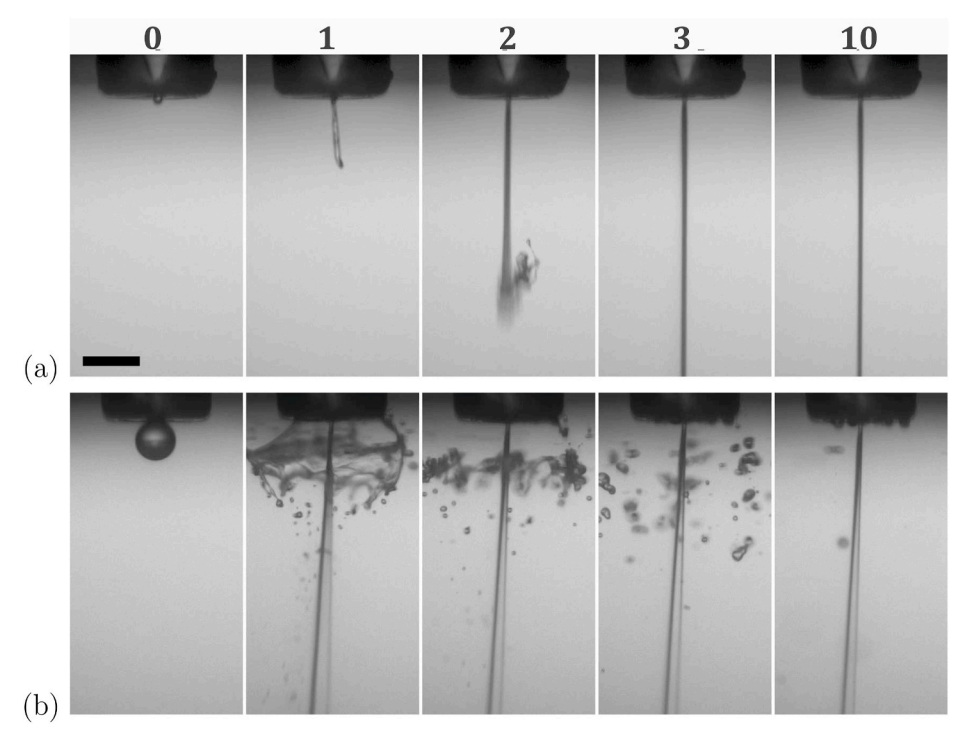


**Fig. 3.** Image sequences from high-speed videos of water jets for (a) P = 0 kPa, and (b) P = -80 kPa. The times in milliseconds from  $t_0$  are shown above each image, and the scale bar in (a) is 2 mm long.

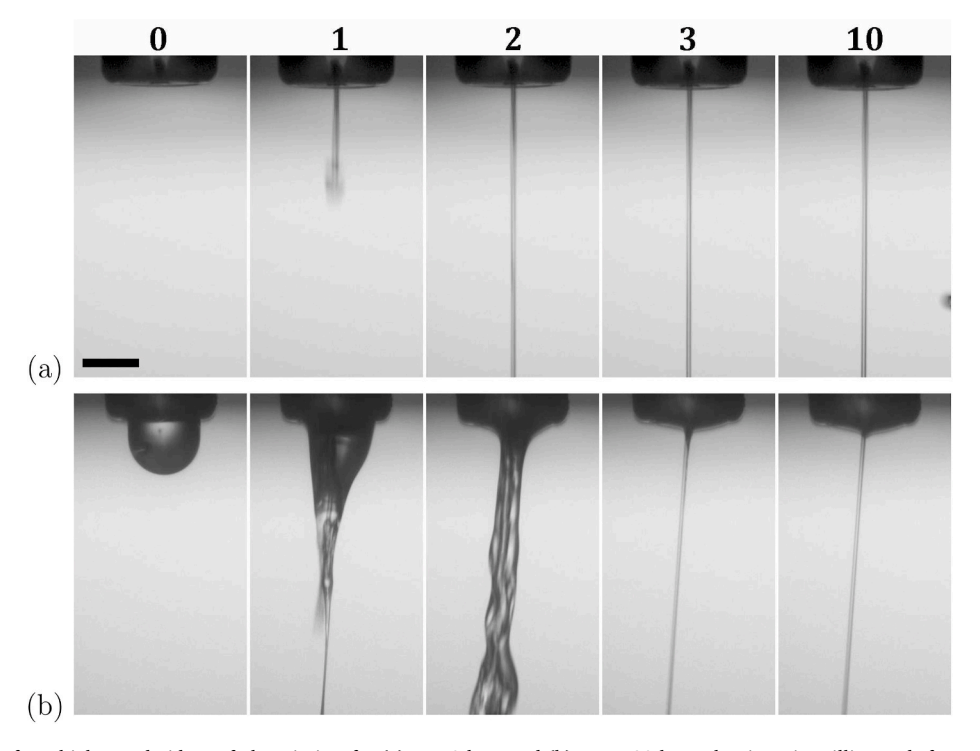


Fig. 4. Image sequences from high-speed videos of glycerin jets for (a) P = 0 kPa, and (b) P = -80 kPa. The times in milliseconds from  $t_0$  are shown above each image, and the scale bar in (a) is 2 mm long.

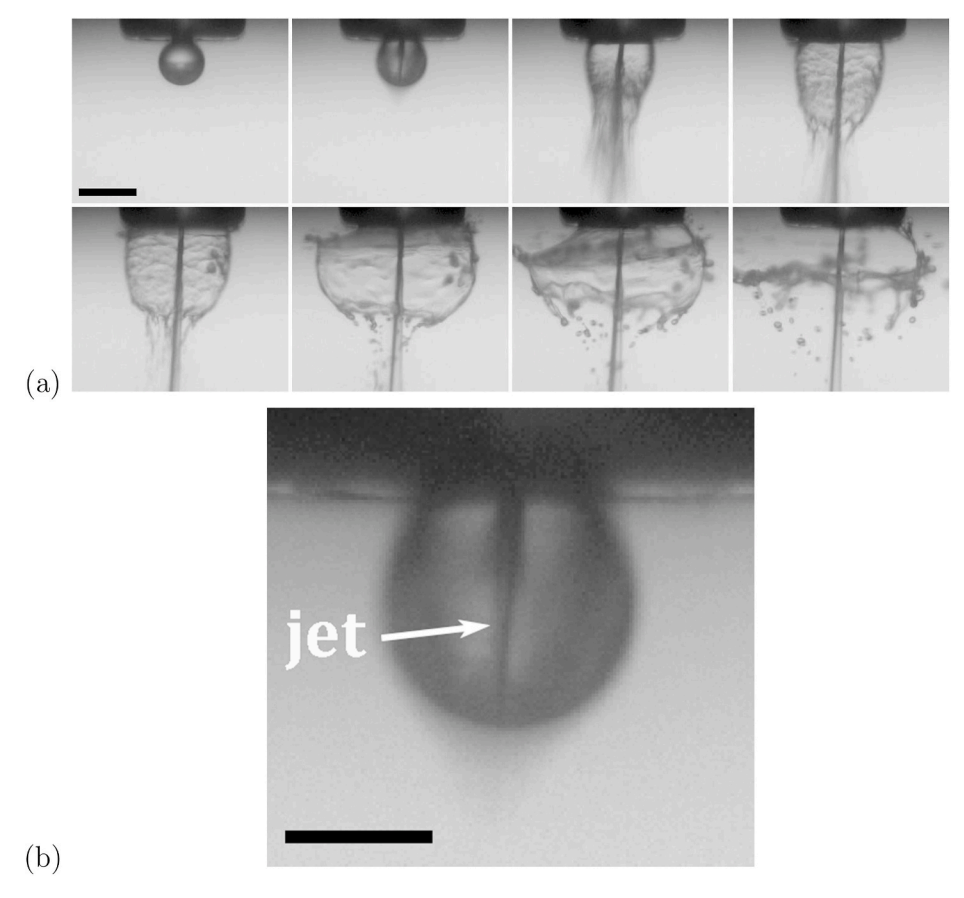


Fig. 5. (a) Start-up sequence for a water jet in P = -80 kPa. The times in microseconds from first motion are t = -62.5, 0, 62.5, 125, 187.5, 500, 812.5, and 1125. (b) Zoomed view of the jet inside the drop during the frame of first detectable motion. The scale bars in (a) and (b) are 2 mm and 1 mm long, respectively.

(image 3). This particular image is reminiscent of the spray caused by focusing a laser pulse into the interior of a pendant or sessile drop [58]. The similarity is due to the pressure impulse that is imparted by the jet (in the present case) and the shock wave from the cavitation event (in the laser pulse experiment). Once the jet pierces the droplet, an annular bell structure forms (images 4 and 5), which is still attached to the cartridge tip. By considering the volume of the pendant droplet, and the surface area of the annular structure, we estimate the thickness of the sheet to be of the order 60– $70~\mu m$ , which is consistent with sizes of the atomized droplets emerging at early times. At  $t \gtrsim 200~\mu s$ , the annular sheet retracts under surface tension away from the cartridge (images 6 and 7) with droplets shedding from the edges, and eventually pulls away into a fluid ring and disintegrates into discrete droplets (image 8). For clarity, a zoomed view of the jet inside the pendant droplet (image 2 in the sequence) is presented in Fig. 5(b).

To understand the role of fluid viscosity in this start-up phenomenon, we present three sequences in Fig. 6 for  $\mu=6.9$ , 215 and 1310 mPa s. The first sequence for  $\mu=6.9$  largely mirrors the dynamics for the water case, the difference of pendant droplet radii notwithstanding. However, as the viscosity increases, the pendant droplet is also observed to increase in size and the phenomena occurs over an exaggerated timescale  $t\sim 5$  ms for  $\mu=215$ . In this case, when the jet pierces the droplet, the fluid viscosity is sufficient to resist the outward inertia imparted by the pressure impulse and collapses back toward the jet, as seen in the second row of images in Fig. 6(b). This leads to a sustained interaction between the sheet and the jet, which persists for several milliseconds.

At the highest fluid viscosity, the jet speed is diminished as compared to lower viscosities, and the effect of the pressure impulse when the jet moves through the drop is less profound. In this case, we therefore observe a steady 'draining' of the droplet, as it is entrained along the jet stream, until  $t \approx 3$  ms, at which point a steady, collimated jet is observed.

To quantitatively assess the jet startup times across the full spectrum of our parameter space, we define  $t_{start}$  as the time from the pressure impulse to the steady jet stream. Our ensemble data for this timescale is presented in Fig. 7, where we observe that there is little effect for pressures  $P \ge -40$  kPa, with  $t_{start} = 0.48-1.2$  ms. However, this range increases to  $t_{start} = 0.73-1.9$  ms for P = -60 kPa, and to  $t_{start} = 1.84-4.6$  ms for P = -80 kPa. As discussed above, and seen in the image sequences, this is due to the interaction between the jet flow and the existing fluid volume pulled through the orifice during depressurization.

Whilst the interaction of the high-velocity jet and the pendant droplet leads to rich dynamics, the ultimate result, within several milliseconds, is a steady jet stream (see Fig. 8), which is collimated for high-viscosity fluids and more disperse for water, due to the turbulent nature of the jet (Re  $\sim O(10^4)$ ). As such, we now proceed to evaluate quantitatively, the effect of pressure and viscosity on the steady jet time and the steady-stream angle and dispersion.

## 3.3. Jetting times

Based upon the fluid dynamics of flow through the orifice, we can write the jet speed in terms of pressure drop as

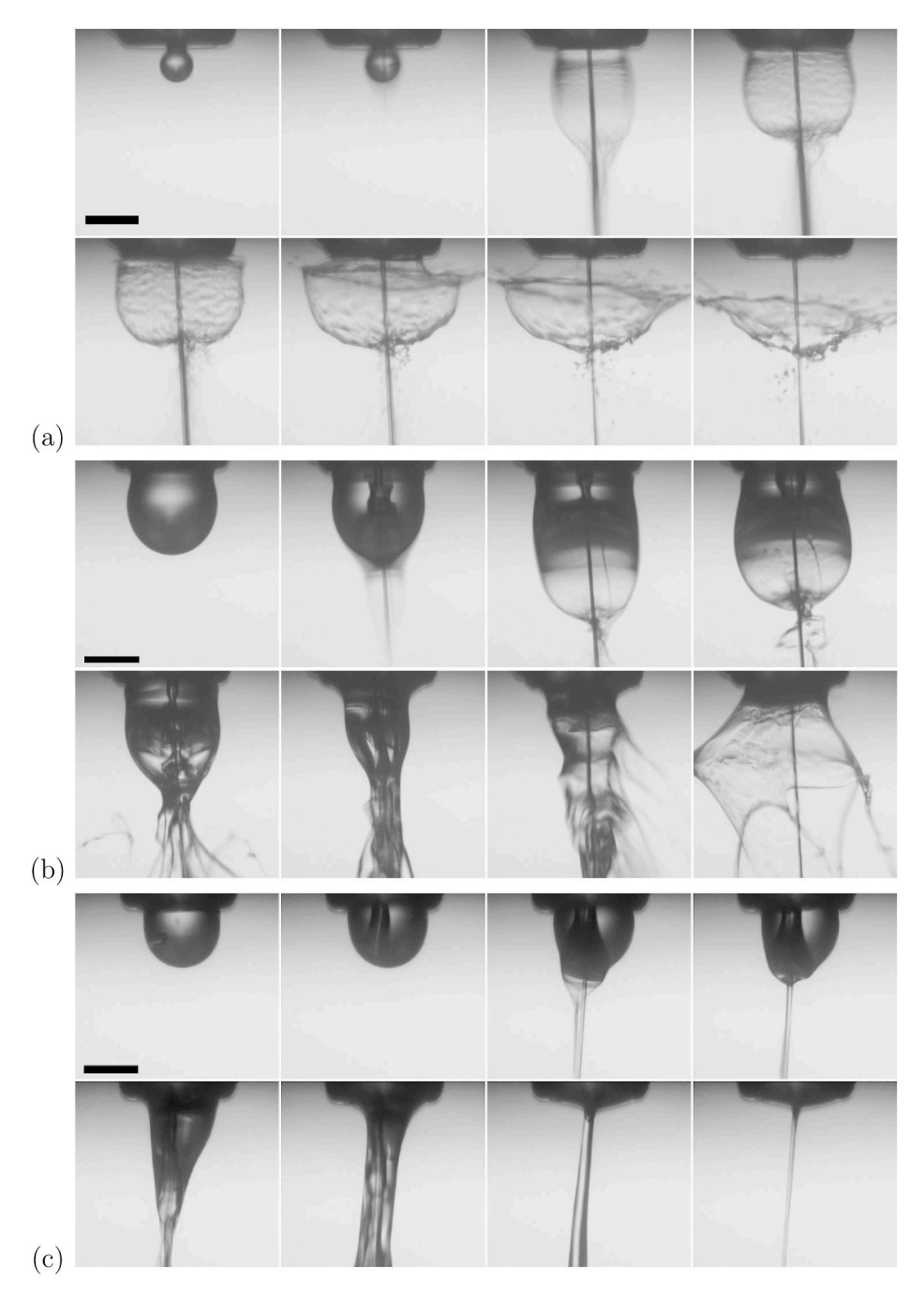


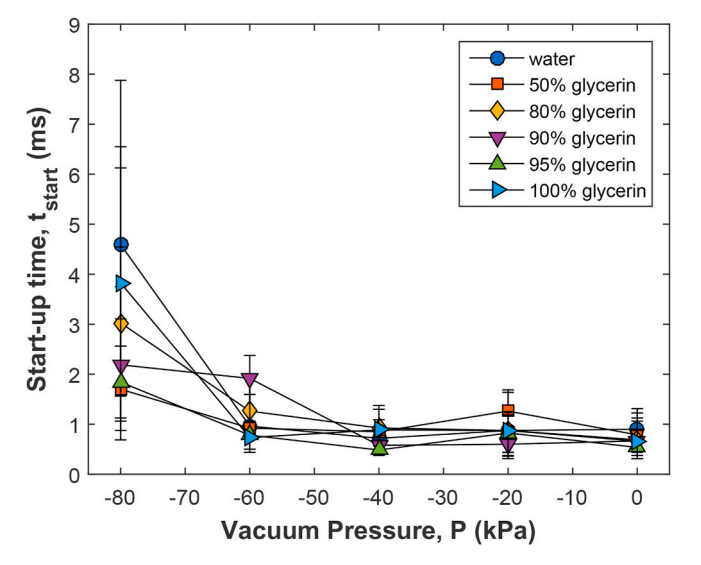
**Fig. 6.** Start-up sequences for (a) 50% glycerin ( $\mu = 6.9$  mPa s), (b) 90% glycerin ( $\mu = 215$  mPa s), and (c) 100% glycerin ( $\mu = 1310$  mPa s), all at P = -80 kPa. In each sequence, the frames are taken at times (relative to first detectable motion) of (a) t = -62.5, 0, 62.5, 125, 187.5, 375, 562.5, and 750  $\mu$ s, (b) t = -62.5, 62.5, 187.5, 312.5, 1062, 2562, 3562, and 5062  $\mu$ s, and (c) t = -125, 0, 125, 250, 937, 1625, 2312, and 3000  $\mu$ s The scale bars are 2 mm long.

$$v_{jet} = \sqrt{\frac{2\Delta P}{\rho(1 + C_d)}} \tag{1}$$

where  $\Delta P=P_0-P_\infty$  is the pressure drop from the upstream cartridge region to the ambient environment, and  $C_d$  is an empirically determined discharge coefficient, which is an increasing function (power law) of viscosity. Since the upstream stagnation pressure is sufficiently high ( $P_0$ )

 $\sim O(10^7)$  Pa) in all cases, we do not expect that the additional pressure drop from the partial vacuum pressure ( $P_\infty \sim O(10^4)$  Pa) will influence the jet speed. To verify this, we inspect the steady jet stream times, i.e. the time from the pressure impulse (e.g. second frame in Fig. 6(a)–(c)) to the end of the jet across all viscosities and pressures. This data is presented in Fig. 9(a), which shows the jet times are largely unaffected by the ambient pressure, but vary significantly with fluid viscosity.

Some of the intra-sample variation in total jetting times at low



 $\begin{tabular}{ll} Fig. \ 7. \ \ Jet \ startup \ time \ versus \ vacuum \ pressure. \ Error \ bars \ encompass \ all \ repeat \ trials. \end{tabular}$ 

pressures can be attributed to the volume loss during the depressurization stage, as exemplified in Fig. 6, where the pendant drops represent an estimated volume loss of 5–10%, resulting in a shorter jetting times in those cases.

By taking the ensemble mean time for each fluid (neglecting effect of pressure), we can now assess the steady jet time versus viscosity, as shown in Fig. 9(b). Here we find that the best description is provided by a power law, given by  $t_j=34+1.34\mu^{0.52}$ . The constant term of 34 ms represents the jet time for an inviscid fluid, whilst the power law exponent reveals the dependence on viscosity,  $t_i^{\sim}\sqrt{\mu}$ .

Previously, average jet speeds have been calculated [54] based on the total jetting time and ejected volume as

$$\langle v_j \rangle = \frac{4V}{\pi D_i^2 t_j} \tag{2}$$

where V is the expelled volume. Taking  $V\approx 100~\mu L$ , which accounts for some fluid loss noted above, we find the jet speeds ranging from 162 m/s for  $\mu=1$  mPa s down to 61 m/s for  $\mu=1310$  mPa s, which are consistent with our calculations from mass conservation, done at atmospheric pressure. Combining equation (2) with the empirical fit for  $t_j$ , we conclude that  $\langle v_j \rangle \sim \mu^{-1/2}$ .

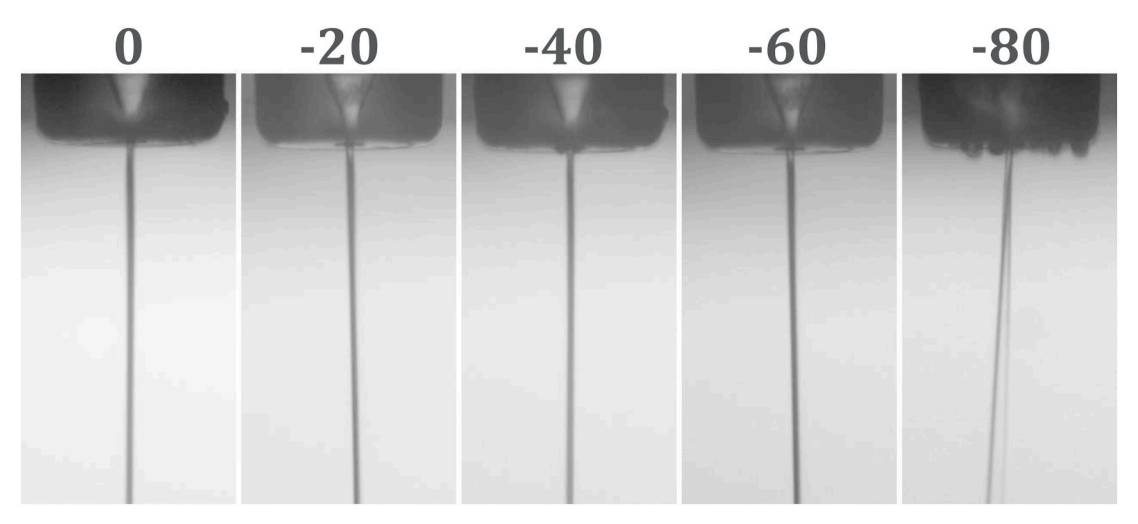


Fig. 8. Snapshots of the steady jet streams for water at all pressures (marked above each image in units of kPa).

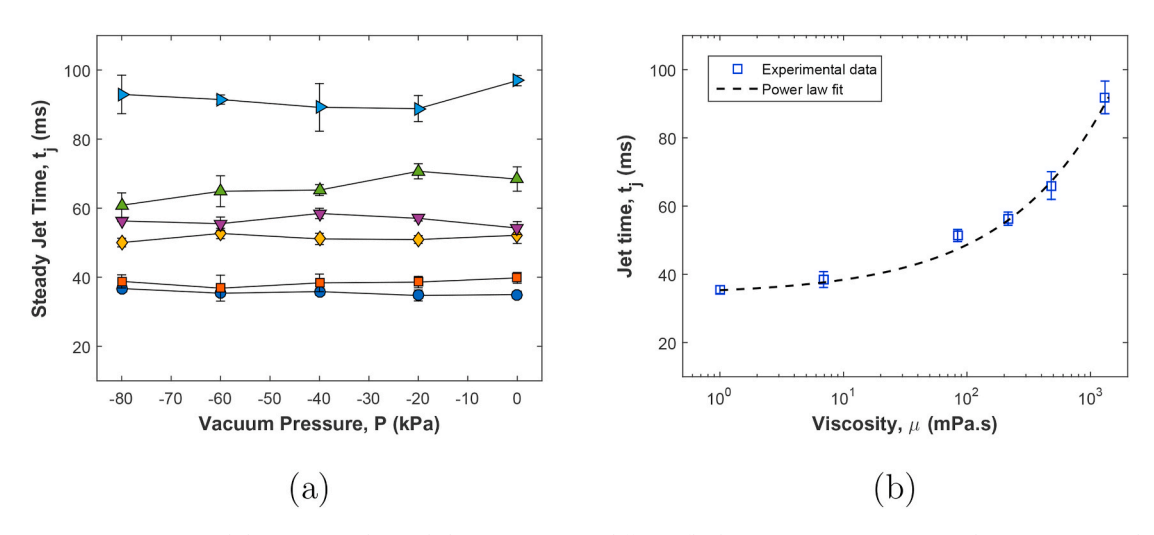


Fig. 9. Jet time versus (a) pressure, and (b) viscosity. The symbols in (a) represent different fluid viscosities: water ( $^{\circ}$ ), 50% glycerin ( $^{\odot}$ ), 80% glycerin ( $^{\circ}$ ), 90% glycerin ( $^{\circ}$ ), 95% glycerin ( $^{\circ}$ ), 100% glycerin ( $^{\circ}$ ). The dashed line in (b) represents the best empirical fit to the data with a power law, given by  $t_j = 34 + 1.34\mu^{0.52}$ .

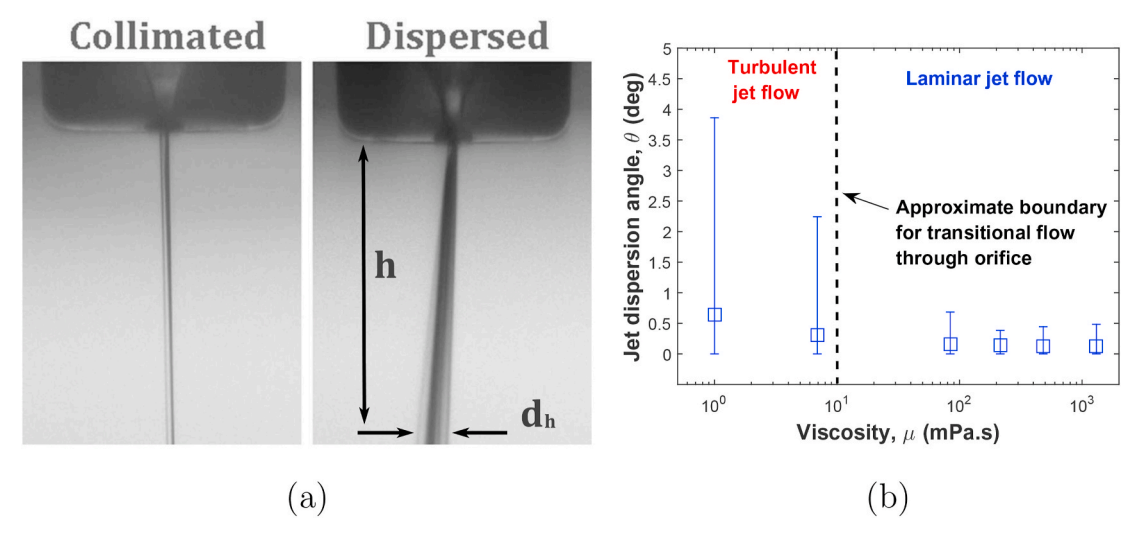


Fig. 10. (a) Examples of both collimated (left) and dispered (right) jets, (b) Jet dispersion angle versus viscosity.

#### 3.4. Jet dispersion

One factor that has the propensity to influence injection quality, in terms of both penetration depth and fluid distribution pattern in the skin, is the jet shape [36,37,44] - namely - whether the stream is collimated or dispersed, as depicted graphically in Fig. 11(a). We can quantify the collimation or dispersion with a jet angle, defined by

$$\theta = \tan^{-1}\left(\frac{D_h - D_0}{2h}\right),\,$$

where h is the distance downstream of the orifice used for measurement,  $D_h$  is the diameter measured at h, and  $D_0$  is the orifice diameter. These are also defined graphically in Fig. 11(a).

As a function of pressure, there is no quantifiable trend for dispersion angle. However, it does appear to be strongly dependent on viscosity, as shown by Fig. 11(b), with dispersion angles up to 4° for water and 2° for 50% glycerin. We note that these fluids result in jet Reynolds numbers,  $Re_j = \rho D_0 v_j / \mu > 25000$  and 3200, which represent fully turbulent and transitional flow, respectively. In contrast, the other fluids with  $\mu = 84 \rightarrow 1310$  mPa s, are strictly laminar with corresponding Reynolds numbers at the orifice of  $Re_j = 2760 \rightarrow 113$ . As such, based upon prior literature [59–61] we expect to observe more fluid dispersion in the case of water and 50% glycerin.

Whilst a dispersion angle of  $1\text{-}2^\circ$  may not seem significant, bear in mind that if a spacer is implemented to impose a stand-off distance of 10 mm between the nozzle and the skin, the jet footprint when it impacts the skin is closer to 1 mm in diameter, which has implications for both fluid splashing, penetration dynamics and subcutaneous distribution patterns. Despite the results of ref [33] where a collimated jet resulted in greater penetration, it reamins unclear whether there is an optimal jet dispersion for intradermal versus subcutaneous or intramuscular delivery. This must be addressed in future studies.

## 3.5. Ex-vivo injections at reduced pressure

To demonstrate the efficacy of injections performed at reduced pressure, we performed a limited number of ex-vivo experiments into Guinea Pig skin. An overview of this approach is shown in Fig. 10, where an orifice stand-off (distance between the orifice and skin target surface) of 2 mm was used. The injected fluid was DI water, for which the jet speed  $v_j \approx 162$  m/s. In this case, due to the small standoff distance, jet dispersion before hitting the skin is minimal with an approximate jet diameter of 250–300  $\mu$ m. The image sequence shown in Fig. 10(a) is from a video taken at 21,000 fps and results in a successful injection into the intradermal region of the skin, evident from the raised skin wheal [62–64] shown in Fig. 10(b). For comparison, figures (c) and (d) present the top and side-views, respectively, for injections performed at P=-80 kPa and 0 kPa; both injection sites appear qualitatively similar and the fluid was correctly deposited into the intradermal tissues. Additional photographs of bleb formations are shown in Fig. 12, for different pressures (indicated at the top) and stand-off distances (indicated on the

It is therefore hypothesized that reduced ambient pressure has a negligible effect on the injection dynamics for low stand-off distances. However, for higher stand-offs this may not be the case due to jet dispersion. As such, it is recommended that in-vivo testing with a clinically relevant animal model be implemented with minimal stand-off.

## 4. Conclusions

In summary, this study reveals that the effect of a negative pressure ambient is virtually negligible with regards to jet times and speeds, which means impulsively started jet injectors are suitable for use with low-pressure environments, and can be coupled with vacuum devices for stabilizing the skin position and tension during injections. One caveat is that for pre-filled cartridges, there is some inherent product loss due to the depressurization, and the fluid present at the orifice can also yield a more dispersed jet during the jet startup phase. This could be circumvented by modifying (increasing) the plunger friction to withstand vacuum pressure. Skin could also be damaged at very low pressures; Therefore we hypothesize that an optimal range of pressures exists for coupling jet injection with vacuum devices, which minimizes skin damage and product loss, but fixes skin location and tension to improve delivery efficiency. Furthermore, direct contact between the orifice and the skin would remove the small amount of product loss due to the

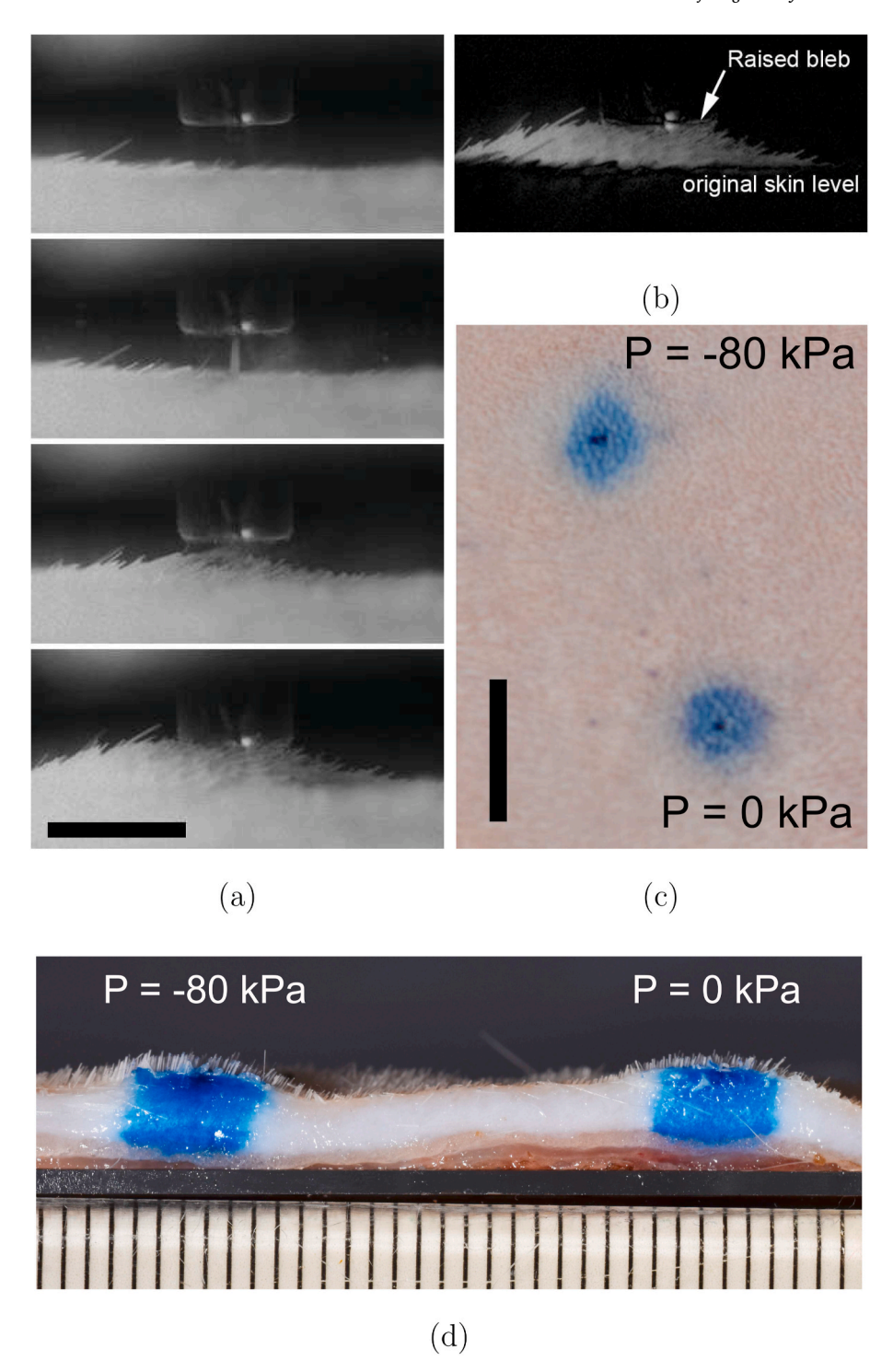


Fig. 11. (a) Jet injection of water into Guinea pig showing the growth of the skin bleb (scale bar = 5 mm). (b) Image difference between original skin level and the final state after injection. (c) Top-view photograph of skin with two injection performed at -80 kPa and 0 kPa, respectively (scale bar = 1 cm). (d) Medial section of the injections showing the fluid dispersion pattern in the dermal tissues (scale is millimetric).

droplet formation.

Whilst the effect of jet dispersion on injection efficiency has yet to be fully quantified, the jet speeds at the orifice remain independent of the vacuum pressure, and are dominated by the high upstream pressure. As such, the dynamic pressure in the jets,  ${}^\sim\!\frac{1}{2}\rho v_j^2$ , remains largely unaffected, and thus the impact pressure,  $P\sim O(10^7)$  Pa, is sufficient for transdermal injection. It is proposed that in-vivo trials using a negative pressure module with a clinically relevant animal model be

implemented with low stand-off to minimize effects of jet dispersion.

#### Author statement

Jeremy Marston and Paul Fisher conceived the project and designed the experiments.

Yatish Rane and James B. Thomas performed the experiments and initial data analysis.

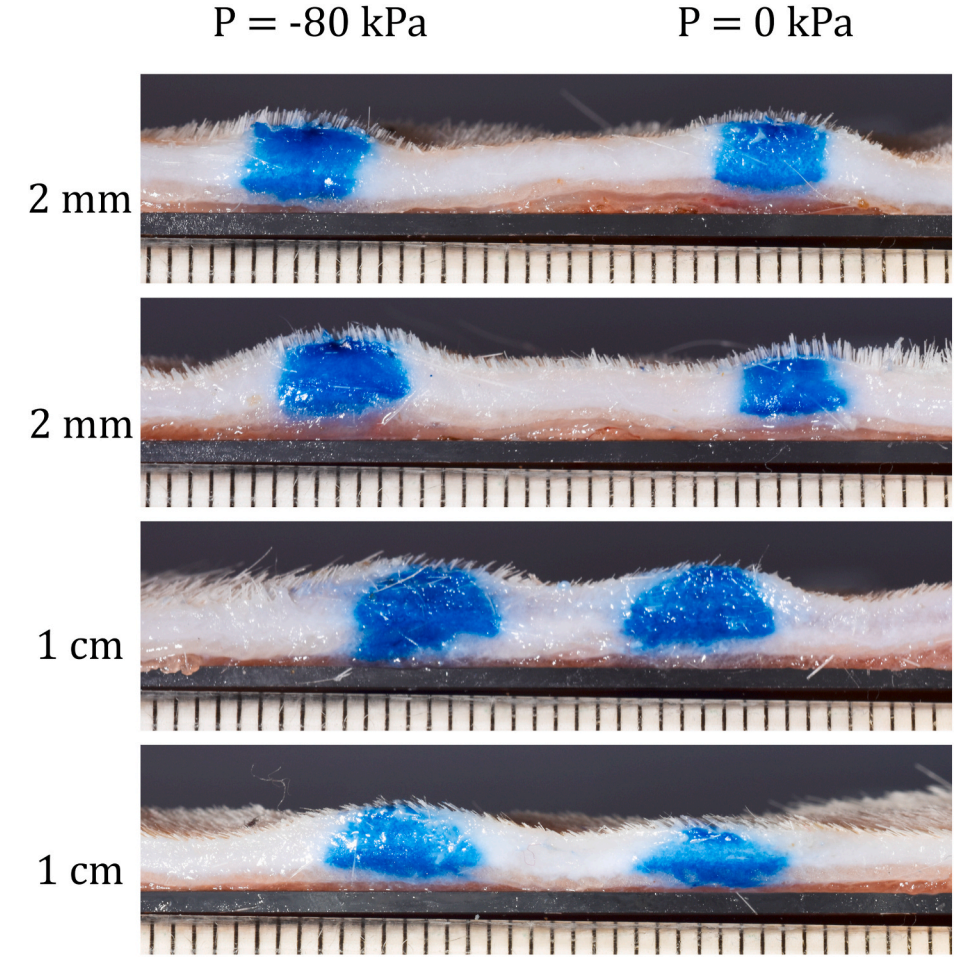


Fig. 12. Photographs of medial sections of the blebs formed from different injection configurations. The scale increments are 1 mm.

Jeremy Marston, Paul Fisher, and Kate Broderick analyzed data. Yatish Rane wrote the original draft, and Final editing was done by Jeremy Marston.

### Declaration of competing interest

The authors declare no competing interest.

# Acknowledgements

This work was financially supported by Inovio Pharmaceuticals and National Science Foundation via award number NSF-CBET-1749382.

## References

- [1] S. Mitragotri, Current status and future prospects of needle-free liquid jet injectors, Nat. Rev. Drug Discov. 5 (2006) 543–548.
- [2] Y. Nir, A. Paz, E. Sabo, J. Potasman, Fear of injection in young adults: prevalence and associations, Am. J. Trop. Med. Hyg. 68 (2004) 341–344.
- [3] G.H. Verrips, R.A. Hirasing, M. Fekkes, T. Vogels, S.P. Verloove-Vanhorick, H. A. Delemarre-Van de Waal, Psychological responses to the needle-free Medi-Jector or the multidose Disentronic injection pen in human growth hormone therapy, Acta Paediatr. 87 (1998) 154–158.
- [4] A. Kane, J. Lloyd, M. Zaffran, L. Simonsen, M. Kane, Transmission of hepatitis B, hepatitis C and human immunodeficiency viruses through unsafe injections in the developing world: model-based estimates, Bull. WHO 77 (1999) 801–807.
- [5] reportThe World Health Report 2002: Reducing Risks, Promoting Healthy Life.
- [6] A. Mannocci, G. De Carli, V. Di Bari, R. Saulle, B. Unim, N. Nicolotti, L. Carbonari, V. Puro, G. La Torre, How much do Needlestick injuries cost? A systematic review of the economic evaluations of needlestick and sharps injuries among healthcare personnel, Infect. Control Hosp. Epidemiol. 37 (2016) 635–646.
- [7] J. Jagger, E.H. Hunt, R.D. Pearson, Estimated cost of needlestick injuries for six major needled devices, Infect. Control Hosp. Epidemiol. 11 (1990) 584–588.

- [8] Dubai, Proceedings of the Annual Meeting of the Safe Injection Global Network, 2010.
- [9] Assessment Report of the Global Vaccine Action Plan, 2014.
- [10] Secretariat Annual Report of the Global Vaccine Action Plan: Monitoring, Evaluation and Accountability, 2016.
- [11] L. Jodar, P. Duclos, J.B. Milstein, E. Griffiths, M.T. Aguado, C.J. Clements, Ensuring vaccine safety in immunization programmes - a WHO perspective, Vaccine 19 (2001) 1594–1605.
- [12] S. Resik, A. Tejeda, O. Mach, C. Sein, N. Molodecky, C. Jarrahian, L. Saganic, D. Zehrung, M. Fonesca, M. Diaz, N. Alemany, G. Garcia, L.H. Hung, Y. Martinez, R. W. Sutter, Needle-free jet injector intradermal delivery of fractional dose inactivated poliovirus vaccine: association between injection quality and immunogenicity, Vaccine 33 (2015) 5873–5877.
- [13] C. Daly, N.A. Molodecky, M. Sreevatsava, et al., Needle-free injectors for mass administration of fractional dose inactivated poliovirus vaccine in Karachi, Pakistan: a survey of caregiver and vaccinator acceptability, Vaccine 38 (2020) 1893–1898.
- [14] A.J. Mohammed, S. Al-Awaidy, S. Bawikar, et al., Fractional doses of inactivated poliovirus vaccine in Oman, N.E. J. Med. 365 (2010) 2351–2359.
- [15] D. Soonawala, P. Verdijk, Wijmenga-Monsuur, C.J. Boog, P. Koedam, L.G. Visser, N.Y. Rots, Intradermal fractional booster of inactivated poliomyelitis vaccine with a jet injector in healthy adults, Vaccine 31 (2013) 3688–3694.
- [16] M.T. Yousafzai, A.F. Saleem, O. Mach, A. Baig, R.W. Sutter, A.K.M. Zaidi, Feasibility of conducting intradermal vaccination campaign with inactivated poliovirus using Tropis intradermal needlefree injection system, Karachi, Pakistan, Heliyon 3 (2017), e00395.
- [17] J. Hickling, R. Jones, Intradermal Delivery of Vaccines: A Review of the Literature and the Potential for Development for Use in Low- and Middle-Income Countries WHO Report, 2009.
- [18] R.A. Hingson, J.G. Hughes, Clinical studies with jet injection: a new method of drug administration, Curr. Res. Anesth. Analg. 26 (1947) 221–230.
- [19] S. Mitragotri, Immunization without needles, Nat. Rev. Immunol. 5 (2005) 905–916.
- [20] E.L. Giudice, J.D. Campbell, Needle-free vaccine delivery, Adv. Drug Deliv. Rev. 58 (2006) 68–89.
- [21] T.R. Kale, M. Momin, Needle free injection technology an overview, Innov. Pharm. 5 (2014) 148.

- [22] M.R. Prausnitz, S. Mitragotri, R. Langer, Current status and future potential of transdermal drug delivery, Nat. Rev. Drug Discov. 3 (2004) 115–124.
- [23] G.E. Theintz, P.C. Sizonenko, Risks of jet injection of insulin in children, Eur. J. Pediatr. 150 (1991) 554–556.
- [24] U. Schneider, R. Birnbacher, E. Schober, Painfulness of needle and jet injection in children with diabetes mellitus, Eur. J. Pediatr. 153 (1994) 409–410.
- [25] K. Benedek, E. Walker, L.A. Doshier, R. Stout, Studies on the use of needle-free injection device on proteins, J. Chromot. A 1079 (2005) 397–407.
- [26] L. Linn, B. Boyd, H. Ointchev, t. King, S.J. Farr, The effects of system parameters on in Vivo injection performance of a needle-free injector in human volunteers, Pharm. Res. 24 (2007) 1501–1507.
- [27] N. Inoue, H. Todo, D. Iidaka, Y. Tokudome, F. Hashimoto, t. Kishino, K. Sugibayashi, Possibility and effectiveness of drug delivery to skin by needle-free injector, Int. J. Pharm. 391 (2010) 65–72.
- [28] S. Hama, M. Arata, I. Nakamura, T. Kasetani, S. Itakura, H. Tsuchiya, T. Yoshiki, K. Kogure, Prevention of tumor growth by needle-free injection of anti-C7orf24 siRNA, Canc. Gene Ther. 19 (2012) 553–557.
- [29] J. Seok, C.T. Oh, H.J. Kwon, T.R. Kwon, E.J. Choi, S.Y. Choi, S.K. Mun, S.-H. Han, B.J. Kim, M.N. Kim, Investigating skin penetration depth and shape following needle-free injection at different pressures: a cadaveric study, Laser Surg. Med. 48 (2016) 624–628.
- [30] J. Schramm-Baxter, S. Mitragotri, Needle-free jet injections: dependence of jet penetration and dispersion in the skin on jet power, J. Contr. Release 97 (2004) 527–535.
- [31] J. Schramm-Baxter, J. Katrencik, S. Mitragotri, Jet injection into polyacrylamide gels: investigation of jet injection mechanics, J. Biomech. 37 (2004) 1181–1188.
- [32] J. Baxter, S. Mitragotri, Jet-induced skin puncture and its impact on needle-free jet injections: experimental studies and a predictive model, J. Contr. Release 106 (2005) 361–373.
- [33] J.C. Stachowiak, T.H. Li, Anubhav Arora, S. Mitragotri, D.A. Fletcher, Dynamic control of needle-free jet injection, J. Contr. Release 135 (2009) 104–112.
- [34] J.C. Stachowiak, M.G. von Muhlen, T.H. Li, L. Jalilian, S.H. Parekh, D.A. Fletcher, Piezoelectric control of needle-free transdermal drug delivery, J. Contr. Release 124 (2007) 88–97.
- [35] A. Taberner, N.C. Hogan, I.W. Hunter, Needle-free injection using real-time controlled linear Lorentz-force actuators, Med. Eng. Phys. 34 (2012) 1228–1235.
- [36] T.M. Grant, K.D. Stockwell, J.B. Morrison, D.D. Mann, Effect of injection pressure and fluid volume and density on the jet dispersion pattern of needle-free injection devices, Biosyst. Eng. 138 (2015) 59–64.
- [37] G. Park, A. Modak, N.C. Hogan, I.W. Hunter, The effect of jet shape on jet injection, in: Proc. 37th Annu. Int. Conf. IEEE Eng. Med & Biol. Soc., 2015, pp. 7350–7353.
- [38] X. Li, B. Ruddy, A. Taberner, Characterization of needle-assisted jet injections, J. Contr. Release 243 (2016) 195–203.
- [39] A. Schoubben, A. Cavicchi, L. Barberini, A. Faraon, M. Berti, M. Ricci, P. Blasi, L. Postrioti, Dynamic behavior of a spring-powered micronozzle needle-free injector, Int. J. Pharm. 491 (2015) 91–98.
- [40] J.W. McKeage, B.P. Ruddy, P.M.F. Nielsen, A.J. Taberner, The effect of jet speed on large volume jet injection, J. Contr. Release 280 (2018) 51–57.
- [41] J.W. McKeage, B.P. Ruddy, P.M.F. Nielsen, A.J. Taberner, Power-efficient controlled jet injection using a compound ampoule, J. Contr. Release 291 (2018) 127–134.
- [42] A. Schoubben, A. Cavicchi, L. Barberini, A. Faraon, M. Berti, M. Ricci, P. Blasi, L. Postrioti, Dynamics behavior of a spring-powered micronozzle needle-free injector, Int. J. Pharm. 491 (2015) 91–98.

- [43] A. Mohizin, K.E.R. Roy, D. Lee, S.K. Lee, J.K. Kim, Computational fluid dynamics of impinging microjet for a needle-free skin scar treatment system, Comput. Biol. Med. 101 (2018) 61–69.
- [44] M. Moradiafrapoli, J.O. Marston, High-speed video investigation of jet dynamics from narrow orifices for needle-free injection, Chem. Eng. Res. Des. 117 (2017) 110–121.
- [45] P. Rohilla, Y.S. Rane, I. Lawal, A. Le Blanc, J. Davis, J.B. Thomas, C. Weeks, W. Tran, P. Fisher, K.E. Broderick, J.A. Simmons, J.O. Marston, Characterization of jets for impulsively-started needle-free jet injectors: influence of fluid properties, J. Drug Deliv. Sci. Technol. 53 (2019) 101167.
- [46] P. Rohilla, J.O. Marston, In-vitro studies of jet injections, Int. J. Pharm. 568 (2019) 118503.
- [47] Y.S. Rane, J.O. Marston, Computation study of fluid flow in tapered orifices for needle-free injectors, J. Contr. Release 319 (2020) 382–396.
- [48] A. Bavdekar, J. Oswal, P.V. Ramanan, et al., Immunogenicity and safety of measlesmumps-rubella vaccine delivered by disposable-syringe jet injector in India: a randomized, parallel group, non-inferiority trial, Vaccine 36 (2018) 1220–1226.
- [49] J.K. Simon, C. Michaela, M.F. Pasetti, et al., Safety, tolerability, and immunogenicity of inactivated trivalent seasonal influenza vaccine administered with a needle-free disposable syringe jet injector, Vaccine 29 (2011) 9544–9550.
- [50] B.S. Graham, M.E. Enama, M.C. Nason, et al., DNA vaccine delivered by a needle-free injection device improves potency of priming for antibody and CD8+ T-Cell responses after rAd5 boost in a randomized clinical trial, PLoS One 8 (2013), e59340
- [51] W. Walther, U. Stein, I. Fichtner, et al., Nonviral jet injection gene transfer for efficient in vivo cytosine deaminase suicide gene therapy of colon carcinoma, Mol. Ther. 12 (2005) 1176–1184.
- [52] Hansen, T.S., Nozzle device with skin stretching means, US Patent 0021716 A1 (2007).
- [53] Cappello, C., Wixey, M., Bingham, J.W., Needle-free intradermal injection device, US Patent 0150820 A1 (2013).
- [54] Slate, J.B., Gorton, L.A. & Burk, M.W., Jet injector, European Patent 1161961 A1 (2002).
- [55] Slate, J.B., Burk, M.W. & Gorton, L.A., Needleless jet injector system with separate drug reservoir, US Patent 55707 A1 (2002).
- [56] Slate, J.B., Burk, M.W. & Gorton, L.A., Needleless jet injector system with separate drug reservoir, US Patent 6,652,483 B2 (2003).
- [57] Slate, J.B., Burk, M.W. & Gorton, L.A., Sequential impulse/delivery fluid medicament injector, US Patent 0059286 A1 (2003).
- [58] S.T. Thoroddsen, K. Takehars, T.G. Etoh, C.-D. Ohl, Spray and microjets produced by focusing a laser pulse into a hemispherical drop, Phys. Fluids 21 (2009) 112101.
- [59] J. Schramm, S. Mitragotri, Transdermal drug delivery by jet injectors: energetics of jet formation and penetration, Pharm. Res. 19 (2002) 1673–1679.
- [60] A. Umemura, Model for the initiation of atomization in a high-speed laminar liquid jet, J. Fluid Mech. 757 (2014) 665–700.
- [61] N. Rajaratnam, C. Albers, Water distribution in very high velocity water jets in air, J. Hydraul. Eng. 124 (1998) 647–650.
- [62] Springhouse, Portable LPN: The All-In-One Reference for Practical Nurses, Lippincott, Williams & Wilkins, Philadelphia, 2005.
- [63] C.C. Dasco, Skin testing for tuberculosis, in: Hall Walker, Hurst (Eds.), Clinical Methods: the History, Physical and Laboratory Examinations, Butterworths, 1976.
- [64] J.A. Simmons, J. Davis, J. THomas, J. Lopez, A. Le Blanc, H. Allison, H. Slook, P. Lewis, J. Holtz, P. Fisher, K.E. Broderick, J.O. Marston, Characterization of skin blebs from intradermal jet injection: ex-vivo studies, J. Contr. Release 307 (2019) 200-210